Joint mechanical properties estimation with a novel EMG-based knee rehabilitation robot: a machine learning approach

Mahdi Bamdad[a,b*], Chiako Mokri[a], Vahid Abolghasemi[c]

[a] Corrective Exercise and Rehabilitation Laboratory, Faculty of Mechanical and Mechatronics Engineering, Shahrood University of Technology, Iran.

[b] Department of Health Science and Technology, Aalborg University, Denmark.

[c] School of Computer Science and Electronic Engineering, University of Essex, UK.

Abstract

Joint dynamic properties play essential roles in a wide range of biomechanical movement control. This paper develops a device with a novel mechatronic design to apply small-amplitude perturbations to the human knee. Surface Electromyography is employed to record such information; at the same time, force and position sensors collect measurements to be sent to identify human joint dynamics. For classification and estimation of force, support vector machine and support vector regression techniques are applied, respectively. We devise a genetic algorithm for parameter optimization and feature extraction within the proposed methods to improve the estimation accuracy. These are then analyzed and compared to the output of our estimation model to provide a reliable comparison. Our extensive experimental results reveal a high estimation accuracy for lower limb muscles to regulate robot impedance parameters. Although the identification method sounds similar to traditional ones, knee joint properties can be estimated by the machine learning approach from the surface Electromyography without perturbations.

Keywords: Knee joint model; Impedance; Rehabilitation robot; Electromyography; Support vector machine

1- INTRODUCTION

Measurement and understanding of the parametric model of joint dynamics as an assessment method of a person's ability and impairment is crucial for implementing proper training plans for rehabilitation users [1-3]. Among the potential biological signals undertaken, electromyography (EMG) is widely used non-invasively. Surveys can produce many mathematical myokinetic models that estimate joint torques from EMG levels[4-5]. EMG-driven musculoskeletal model by accounting for the muscle properties could improve joint stiffness estimation [6-7], and it has been successfully used to characterise the control strategies such as impedance control [8-11]. At the same time, sEMG is affected by physiological factors such as phase neutralization and improper placement of electrodes. These factors subsequently affect the accuracy of force or joint properties modeling [12].

Raw sEMG signals can also be easily affected by other external factors such as motion artifacts, ambient noise, and electrical equipment noise. In this regard, various techniques devise pre-processing methods [13]. After a pre-processing stage, the input signal is typically categorized into several classes (both for classification or estimation) depending on the tasks performed by subjects during the signal acquisition. Different modeling techniques have been used to accurately estimate muscle strength using EMG signals, including wavelet [14], artificial neural network (ANN)[15-16], and support vector machine (SVM)[17]. In particular, knee torque could be estimated by a support vector regression (SVR)[18-19], some with a specific application in the control of robotic rehabilitation[20]. One of the main challenges in using SVR-based techniques is model parameter selection. Instead, the optimisation methods could calculate the parameters of the backup vector regression method [21].

This study has explored a reliable method to execute impedance modulation from EMG, which is necessary for the parameter tuning of rehabilitation robot control to guarantee high performance with safety. We discussed a low-cost robotic system with a novel human-machine interface. In addition to the conventional robotic functions, an instrumented tool system is operable to address joint model identification. We have demonstrated a powerful technique to establish a measurement of personalized joint properties within this human-in-the-loop machine learning. Nonetheless, the classification accuracy for obtaining the knee joint dynamic parameters is crucial. We identify a potentially nonlinear joint dynamic model with the fewest terms required to describe how the measurement sEMG signal changes for each subject. The main contributions are outlined below:

- Designing and implementing a new 1-DOF knee rehabilitation robot that combines a joint-driving assistive device for identification with typical functions of knee therapy.
- Recording of sEMG and force signal simultaneously with the designed protocol at any arbitrary angle of knee movement (both isometric and isokinetic).
- Impedance characterization in functional tasks for the knee joint. It would take a step further along with the realizing a measurable safe interaction.
- Using suitable features from the input signals to improve the EMG classification accuracy in joint model estimation to increase the performance of knee therapy.

The rest of the paper is organized as follows. Section II represents the Apparatus system and implementation details, including the rehabilitation device specifications with mechatronic design. Section III will describe data recording, experiment method, and protocol. In Section IV, the acquisition process and the proposed machine learning technique will be discussed. This section is devoted to providing an approach for model selection and parameter optimisation. Section V will formulate and synthesize the knee joint dynamics for impedance parameter identification. Section VI is devoted to the experimental results on both classification and prediction in this research. Finally, the paper is concluded in Section VI.

2- DESIGN AND IMPLEMENTATION OF A KNEE REHABILITATION ROBOT

The architecture of one degree of freedom rehabilitation manipulator is shown in Fig. 1. Experiments should be done on a testbed that can isolate and focus only on one quadriceps muscle group. This work aimed to design a sitting-type lower limb rehabilitation robot. Although the primary motivation for developing this robot is rehabilitation, it can be used to accurately predict joint dynamics in biomechanics with application in robotic therapy control.

2-1- Hardware configuration

A single-joint training is usually chosen for a specific range of motion exercise. A calibrated scaled arc with angles of 30, 60, and 90 degrees is installed, and the pointer fixes the motion for isometric tests. The hardware control system contains the central motion control module, a simple interface for EMG signals, and the sensor feedback system based on the required functions. The leg extension/flexion device is connected to a personal computer for signal capturing, conditioning, feature extraction, and classification. The actuator element is a Faulhaber DC Motor (24V, 220W)

that could generate an angular position precisely. Speed controller allows controlling the motor direction using a Pulse-Width-Modulated (PWM) DC voltage with a Duty Cycle fully adjustable from 0%-100%. It provides a ramp torque response with a continuous current to the motor, and the actuator delivers a controllable perturbation correspondingly.

Figure. 1: Device and components- knee rehabilitation robot with annotated details.

2-2- Sensory System

The joint mechanical impedance is commonly measured dynamically by applying perturbations about a joint at a fixed operating point. As such, we know quantifying torque change vs. angle change by accurate measurement and, on the other hand, analysis of joints' range of motion is essential in the experiment analysis. The bulky, expensive devices such as dynamometers could impose movements, but time-consuming calibration tasks and examination protocols that differ too much from the qualitative clinical examination are severe concerns.

This section describes a calibrated wearable inertial measurement unit (IMU) built with a pair of triaxial accelerometers, as shown in Fig. 2(a). To ensure that the sensor coordinate is aligned with the body planes of the shank and thigh, calibration prior to the experiment was arranged. Determining knee angle without the need for integration could reduce the effect of offset drift [22-23].

We use two IMUs placed on the patella of the joint, in the central bone axis at two radii from the knee joint. The MPU6050 IMU has both a 3-Axis accelerometer and a 3-Axis gyroscope integrated on a single chip in connection with Arduino Board. For accurate estimations of angles as well as angular velocities, the two estimates are fused using a complementary filter. Our results approve that we have an ignorable drift error. Besides having a scaled arc that is mechanically adjusted at a pointer at a certain angle, due to having more viable data, a Kalman filter was used to estimate the error states of the IMU. Finally, the vector algebra algorithm is also used to calculate the angle between two accelerometer readings. It may be calculated as follows [24]:

$$\varphi = \cos^{-1}\left(\frac{a_{x1}a_{x2} + a_{y1}a_{y2} + a_{z1}a_{z2}}{\sqrt{a_{x1}^2 + a_{y1}^2 + a_{z1}^2}\sqrt{a_{x2}^2 + a_{y2}^2 + a_{z2}^2}}\right) \quad (1)$$

where a_{xi} , a_{yi} , a_{zi} are the X, Y, Z components of acceleration of ith accelerometer. As an alternative formulation, when we lose some data, mainly occurring in the Z-direction, we can follow this [25]:

$$\varphi = \tan^{-1}\left(\frac{a_{y1}a_{x2} - a_{x1}a_{y2}}{a_{x1}a_{x2} - a_{y1}a_{y2}}\right) \quad (2)$$

We receive force data from a load cell (shear beam model-SEWHA-SB210) followed by an A/D converter (HX711). As shown in Fig. 2(b), the load cell's mounting and location also play an essential role in measuring muscle strength accurately. The sensor is attached to the linkage while rotary support is connected to the robotic arm. This design aims to collect more reliable force data and guarantee safe contact between the leg and the force sensor.

Figure. 2: The architecture of sensory system (a) wearable IMU arrangement (b) force sensor (load cell).

3- MATERIAL AND METHODS

3-1- sEMG Data recording

Prior to the experimental trials, isometric maximum voluntary exertions (MVE) in knee extension and knee flexion were recorded during three repeated 5s trials. The perturbation could be achieved by the control technique implementation of a single-axis actuator module during the recording. Skin cleansing is essential to reduce sensing impedance. During these measurements, to make a portable experiment, an 8-channel EMG device has a power bank to supply 5-volt power to the device. As shown in Fig. 3, Ag-AgCl surface electrodes were also used for recording the electrical activity produced by three quadriceps muscles: Vastus medialis (VM), Vastus Letralis (VL) and Rectus femoris (RF), with 1 kHz sampling frequency.

Figure. 3: Electrode locations: (1) Rectus femoris; (2) Vastus medialis; (3) Vastus lateralis; (4) Zero reference electrode.

3-2- Experimental method

According to the approved protocol, all volunteers were subjected to sEMG analysis and examined in the Corrective exercise and Rehabilitation Laboratory, supervising clinical faculty mentors. Five healthy subjects (males, aged 21-30 years) were asked to place their right foot in the foot clamp to

ensure it was fixed. During the exercise, the person was asked to apply force to the load cell for 5 seconds to relax and open the knee, and rest for 5 seconds. Individuals' age and height characteristics were measured, and their mean and standard deviation were 23.5±4.5 years and 174.10±4.3cm, respectively.

3-3-Joint dynamic model

Knee dynamics which is expressed as the relationship between joint torque and angular displacement, is quantified using limb inertia, joint stiffness, and viscosity[26]. Our approach involves applying small position perturbations $\delta\varphi$ to the joint trajectory φ_0 as

$$\varphi(i,t) = \varphi_0(i,t) + \delta\varphi(i,t) \tag{3}$$

The estimated joint torque can be computed from the sum of the partial torque contributions provided by the human muscles to push the robotic link, as shown in Fig. 2(b). After calculating the actual joint angle φ, then we apply mathematical models for the overall effective torque T_e around the joint

$$T_e = T_R(\varphi,\dot{\varphi},\ddot{\varphi}) + \underbrace{T_0 + T_P}_{Human} \tag{4}$$

where T_R is the robotic link component, and T_0, T_P are two terms from the human side. The torque component produced by the passive knee mechanism is T_0 due to φ_0. Also, T_P is a perturbation torque, produced by the intrinsic and reflex responses to the position perturbation $\delta\varphi$[27].

3-3-1- Torque components:

The passive knee mechanism torque T_0 may be measured through s-EMG while the robot driving joint is not supported. This model could relate EMG to torque by the average rectified EMGs for each isometric contraction. It contains T_{ext}^{EMG} only the values for the extensor muscles, and T_{flex}^{EMG} for the flexors as:

$$T_0 = T_{ext}^{EMG} + T_{flex}^{EMG} \tag{5}$$

The net torque predictions based on EMG measurements closely matched the net torque measured by the force sensor in all conditions. Perturbation torque T_P might be estimated from measurements of overall joint torque in three steps. (1) a steady joint trajectory is exerted, and the

load cell records the forces, includes the human torque T_0 . (2) a perturbed joint trajectory is then applied, and the overall human torque is recorded. (3) after the computation of torque difference in both experiments, the perturbation torque can be estimated.

The contributions to joint torque T_R due to HRI control can be described using an inverse dynamic Newton-Euler model formulation, similar to the modeling of robots

$$T_R = \left(\frac{m_1}{3} + m_L\right) L_e^2 \ddot{\varphi} + \left(\frac{m_1}{2} + m_L\right) L_e g_0 \cos(\varphi) + b(\dot{\varphi}) \tag{6}$$

where m_1 the mass distribution of the link, including the human leg and m_L is the effective mass at the end of the rotary link. Considering the gravitational contribution g_0, in technical terms of $b(\dot{\varphi})$, the first-order derivative $\dot{\varphi}$ is involved in the nonlinear terms (e. g. viscous friction, damping) explicitly in the dynamic system. We can neglect the nonlinear terms in this single link robotic arm. Therefore, the state space equation can be written as:

$$\begin{cases} \dot{\varphi} = \upsilon \\ \dot{\upsilon} = \dfrac{T_R - L_e g_0 \cos(\varphi)\left(\dfrac{m_1}{2} + m_L\right)}{\left(\dfrac{m_1}{3} + m_L\right) L_e^2} \end{cases} \tag{7}$$

3-3-2- IBK Model

The intrinsic model is often described by a second-order model having inertia (I), viscosity (B), and elasticity (K). The second-order mechanical model (IBK model) has been used as:

$$T_P(i,t) = I(t)\delta\ddot{\varphi}(i,t) + B(t)\delta\dot{\varphi}(i,t) + K(t)\delta\varphi(i,t) \tag{8}$$

The system of equation (8) can be solved by the standard least square method through standard matrix form as :

$$Y(t) = X(t)\beta(t) \tag{9}$$

$$Y(t) = \lfloor T_P(1,t) \cdots T_P(N,t) \rfloor^T$$
$$\beta(t) = \lfloor I(t), B(t), K(t) \rfloor^T$$
$$X(t) = \begin{bmatrix} \delta\ddot{\varphi}(1,t), \delta\dot{\varphi}(1,t), \delta\varphi(1,t) \\ \vdots \\ \delta\ddot{\varphi}(N,t), \delta\dot{\varphi}(N,t), \delta\varphi(N,t) \end{bmatrix}.$$

Assuming that $\delta\varphi$ and the relevant differential terms have been obtained through the ensemble method and the ensemble of N is used in the least square method. Moreover, the low-pass filter could be applied for a well-damped condition to avoid a resonance effect.

$$L(s) = \frac{a^n}{(s+a)^n} \tag{10}$$

To simplify the explanation of applying filter, time and frequency representations are mixed as:

$$L(s)I(t)\delta\ddot{\varphi}(i,t) = \int_0^t h(t-\varepsilon)I(\varepsilon)\delta\ddot{\varphi}(i,\varepsilon)d\varepsilon \tag{11}$$

where $h(t-\varepsilon)$ is the impulse response function of *L(s)*. Also, *I(t)* can be taken out of the integration as:

$$L(s)I(t)\delta\ddot{\varphi}(i,t) \approx I(t)\frac{a^2}{(s+a)^2}s^2\delta\varphi(i,s) \tag{12}$$

According to the main IBK model equation in (6), the third term does not need any manipulation, and it could be rewritten as:

$$\frac{a^2}{(s+a)^2}s^2T_P(i,s) = I(t)\left[a^2 - \frac{a^2(2as+a^2)}{(s+a)^2}\right]\delta\varphi(i,s) + \left(B(t)s + K(t)\right)\frac{a^2}{(s+a)^2}\delta\varphi(i,s) \tag{13}$$

The operations of $\delta\varphi$ with low-pass filters could achieve I(t), B(t), K(t) as the output parameters in the experiment [28].

3-4- Pre-processing Module

The recorded EMG data and the measured force by the load cell should be used as the input and output of the proposed models. Both raw EMG and force signals are easily contaminated by external factors such as electrode noise, motor artifacts, transmission line noise, and ambient noise. Therefore, it is crucial to remove or mitigate the effects of unwanted noises and artifacts before the central processing stage. We follow standard state-of-the-art pre-processing techniques to remove

unwanted noise and artifacts. For instance, low frequencies 1-20Hz, which do not involve important information and are corrupted by movement artifacts, will be rejected. Radiation from power sources, also called Power-Line Interference, is an ambient noise arising at 50 or 60 Hz. The impact of this noise can be mitigated by applying a narrowband notch filter. Overall, the pre-processing stage prepares the EMG and force signals according to Figs. 4 and 5, respectively.

3-5- Machine Learning Module

Support vector machine is a supervised learning method used for classification and regression. The basis of SVM classification is linear data separation, where a hyperplane separates samples of the different classes. SVM transforms the input data points into a feature space that can be linearly separated. What makes the support vector machine different from other classifiers is how it selects the hyper-plane. In a support vector machine, the objective is to find the maximum margin between the two classes. The decision-making function for separating data is determined by a subset of the closest training data to the hyper-plane, called support vectors. The optimal hyperplane in a support vector machine is a separator between support vectors. Due to the simplicity and flexibility of SVM, we are interested in applying it for sEMG classification. Although SVM can be used to classify the subject's state, it cannot be used to evaluate the system performance based on the measured muscle force. Also, SVR can be used in this regard as it solves predictive and estimation problems [29]. To use the support vector machine in regression problems, Vapnik [30] used a loss function that ignores errors at a certain distance from the actual values. In SVM regression, the input x is first mapped onto a feature space using fixed nonlinear mappings, and then a linear model is constructed in this feature space. Using mathematical notation, the linear model in the feature space is given by

$$f\left(x,w\right)=\sum_{j=1}^{m}w_j g_j(x)+b \tag{14}$$

where b is the bias term and $g_j(x), j=1,...,m$ denotes a set of nonlinear transformations. Here, the bias term could be dropped as the data are assumed to be zero mean, achieved by preprocessing. The loss function called ε-insensitive is then defined as follows:

$$L\left(y, f\left(x,w\right)\right)=\begin{cases}0 & if\ \left|y-f\left(x,w\right)\right|\le\varepsilon\\ \left|y-f\left(x,w\right)\right|\le\varepsilon & otherwise\end{cases} \tag{15}$$

Figure. 4: EMG pre-processing example for subject 1 (S1) and Rectus Femoris: (a) Raw EMG, (b) DC removal, (c) Spectrum signal, (d) Butterworth High pass filtering, (e) Butterworth Low pass filtering, (f) Notch filtering, (g) Rectification, (h) Smoothing, (i) Normalization.

Figure. 5: Force signal pre-processing: (a) Raw signal, (b) Butterworth filtering, (c) Notch filtering, (d) Rectification, (e) Smoothing, (f) Normalization.

SVM regression performs linear regression in the high-dimension feature space and needs to reduce model complexity by minimizing $\|w\|^2$. The optimal regression function can be defined by minimizing the following function:

$$Min\ \frac{1}{2}\|w\|^2+C\sum_{i=1}^{n}\left(\xi_i^-+\xi_i^+\right)$$

$$subject\ to\begin{cases}y-f\left(x_i,w\right)\le\varepsilon+\xi_i^+\\ f\left(x_i,w\right)-y_i\le\varepsilon+\xi_i^-\\ \xi_i^-,\xi_i^+\ge 0, i=1,...,n\end{cases} \tag{16}$$

where C is a predetermined value, and ξ_i^- and ξ^+_i are slack variables that determine the upper and lower constraints of the system output. This optimization problem can be transformed into a dual problem and its solution is given:

$$f\left(x\right)=\sum_{j=1}^{n_s}\left(\alpha_i-\alpha_i^*\right)K\left(x_i,x\right) \tag{17}$$

$$subject\ to\begin{cases}0\le\alpha_i^*\le C\\ 0\le\alpha_i\le C\end{cases}$$

where n_s is the number of support vectors and the kernel function

$$K\left(x_i,x\right)=\sum_{j=1}^{n_s}g_j(x)g_j(x_i) \tag{18}$$

Selecting a particular kernel type and kernel function parameters is usually based on application-domain knowledge and also should reflect the distribution of input values of the training data.

FEATURE EXTRACTION AND PARAMETER OPTIMIZATION

3-6- Feature extraction in SVM/SVR based on GA

There are two significant challenges in maximizing the performance of EMG classification: i) selecting the most appropriate features and ii) optimising the tunable parameters. Genetic algorithm (GA) as a meta-heuristic technique has been used successfully and extensively to select the optimal model parameters in support vector machines [31]. The SVM model is formed using the training data with calculated parameters for desired hyperplanes. To calculate the objective function, the test data is classified by the trained SVM model, and an error matrix is formed. After evaluating the members in GA, three steps of selection, integration, and mutation are performed on the binary format of the parameters, and a new population is generated. These steps are repeated to establish the stopping condition. Details of this process have been depicted in Fig. 6.

Figure. 6: The proposed flowchart for SVM-GA.

To define a criterion for evaluating the quality of a subset of selected features, two parameters of classification accuracy and the number of features chosen N_f must be considered. In other words, the desired classification would include the subset of the most effective attributes as well as a lower number of selected features. Therefore, we maximise objective function f by representing these two criteria in:

$$f = W \times Accuracy + (1-W) \times \frac{1}{N_f} \tag{19}$$

where W as the weights in range of [0,1] controls the contribution between the number of features and classification accuracy. Then three selection, merging and mutating operators act according to the quality of each member. This process is repeated to establish a stopping condition.

3-7- Parameter Optimization Using GA

Selection of the optimal parameters for machine learning techniques is a challenging task. Here, there are two sets of parameters to be identified: i) adjustment parameters that mainly balance the error and complexity minimization of the model (e.g., C), and ii) kernel parameters. Among various kernels for the support vector machine's regression model, the radial basis function

(RBF) kernel showed a more appropriate result for predicting:

$$K(x_i, x) = exp\left(-\frac{\|x_i - x\|^2}{2\sigma^2}\right) \quad (20)$$

Hence, σ is the most crucial unknown parameter in RBF kernel which require to be found. As depicted in Fig. 7, we propose a GA-based technique to select the optimal parameters automatically. The so-called model selection approaches in this context are divided into two categories. In the first category, the same set of parameters is considered for all classes. While in the second category, different parameters are determined for each class. To properly evaluate the quality of any member in GA, we convert both parts of the chromosome to a real number. The support vectors for both SVM/SVR will be formed by using the training data as well as the tuned parameters of the corresponding hyper-planes. Then, the test data is given to the obtained model in the training step, and an error matrix is formed. After evaluating the samples, three steps of selection, integration, and mutation are performed on the binary format of the parameters, and a new population is created. These steps are repeated to establish the stopping condition.

Figure. 7: Diagram of the layout and steps of this process, including EMG signal acquisition, processing, force feedback and the regression model.

4- EXPERIMENTAL RESULTS

4-1- Machine Learning performance analysis

In the first experiment, we aim to assess the performance of SVM for all five subjects. As a well-established performance measurement technique, we have used K-fold cross-validation in all our experiments. Hence, the results of Table 1 are obtained according to K-fold cross-validation with K=10. To further assess the effectiveness of the proposed model, the details of performance evaluation per each fold are provided here. Such analyses demonstrate the generalizability power of the model for new or unseen data [32]. In the K-fold cross-validation technique, the entire dataset is divided into two complementary sub-datasets, i.e. training and testing. Then, for each model, i.e., SVM, SVM-GA, and SVM-GA-F, the dataset is first randomized and then partitioned (split) into K almost equal-sized sub-datasets called folds [32].

Then, K-1 folds participate in training and 1 fold is considered for testing. This process is repeated for K times such that sub-sets are included in the training and testing. Fig. 8 depicts an illustrative view of this process. Mean Square Error (MSE) and Relative Standard Error (RSE) could be considered to determine the robustness of the algorithm as:

$$MSE = \frac{1}{n}\sum_{i=1}^{n}(\hat{Y}_i - Y_i)^2$$
$$RSE = \sqrt{\frac{\sum_{i=1}^{n}(\hat{Y}_i - Y_i)^2}{\sum_{i=1}^{n}(\overline{Y}_i - Y_i)^2}}, \overline{Y} = \frac{1}{n}\sum_{i=1}^{n} Y_i \quad (21)$$

where Y is the original signal, and $\hat{Y}$ is the estimated signal through n samples. Table 1 presents the calculated MSE and RSE. The accuracy for all three models per fold are reported and it confirms that the proposed method performs robustly across different data folds:

Figure. 8: K-fold cross-validation representation with K=10

Table 1: Performance evaluation of the proposed model using 10-fold cross-validation. Each row shows the results when 1 fold is used for testing and the remaining for training.

For all five subjects given in Table 2, the average classification accuracy of 93.14% has been achieved. Fig. 9(a) illustrates the confusion matrix of the classifier's output (for subject S1) with respect to the target class. Values in the green boxes show the percentage of the associated class data for the total data. For example, it can be seen from Fig. 9(a) that out of 4568 samples in class 0 (equivalent to 43.5% of total data) 91.4% has been predicted correctly. Also, out of 432 samples in the same class (equivalent to 4.1% of total data), 8.6% has mispredicted. The same interpretation can be made for the results of class 1 in Fig. 9 (a). In the next experiment, we aim to observe the effects of using optimised SVM parameters by GA on our experiment's data. In the proposed genetic algorithm, the main population was chosen as 20, with performing 50 iterations of the target function. Fig. 9(b) shows the confusion matrix associated with the SVM-GA results with $C = 2$ and $\alpha = 1.5$ (obtained by GA) on S1. It is seen that when the specified conditions are fulfilled, the average accuracy meets 96.6% which is higher than the previous experiment.

Figure. 9: Confusion matrix result for S1 with various classification methods.

Figure. 10: Comparison of classification accuracy using direct samples (SVM) and selected features (SVM-F).

Table. 2: Classification accuracy for all five subjects.

To explore how GA can affect classification performance, another experiment was conducted. The same GA settings in the previous experiment are also considered here. The results of two cases are presented in Fig. 10; i) data samples with all features are used for classification (SVM), and ii) selected features via GA are used for classification (SVM-F). As observed from Fig. 10, the classification accuracy increases when selected features by GA are used by SVM.

It is noted that selecting the weights, one for each feature is one part of the iteration process of optimization. Instead, the selection of parameters C, and α will automatically achieve the optimized values for weights [18][33]. From Table. 2, applying SVM with selected features and optimized parameters C, and α using GA shows a better performance. All subjects are independent and there is no relationship among them. It can be noticed from the columns that we have sorted the accuracy from higher to lower and renumbered the subjects.

It demonstrates the average performance of various SVM techniques across the subjects, SVM with no feature selection (SVM), SVM with optimised parameters (SVM-GA), SVM with optimised parameters, and selected features (SVM-GA-F). The average classification accuracy by SVM-GA-F reached 96.7%, which is even higher than SVM-GA.

To evaluate the performance of both SVR and SVR-GA, two different approaches are adopted. In Approach A, two data trials were collected from each subject, where one was used for training and the other used for the testing phase. In Approach B, 70% of both trials from each subject were considered for training, and the remaining 30% were included in the test. We performed 10-fold cross-validation to select these data partitions randomly while the low values of K result in a noisy estimate of model performance.

In both experiments, RBF kernel with $\varepsilon = 0.3$, $C = 0.5$, and $\sigma^2 = 3$ was selected for the regression model. Parameter C determines the trade off between the model complexity (flatness) and the degree to which deviations larger than ε are tolerated in optimization formulation. Choosing large (infinity) C, minimize the loss function in Eq. 15, without regard to model complexity part in the optimization formulation. Fig. 10 illustrates the estimated and measured force signals of S1 using approach A in both SVR and SVR-GA methods. These results show high accuracy of the estimation process as well as small RMSE. Notably, a significant improvement in reconstruction error and estimation accuracy can be observed for SVR-GA in Fig. 10(c) and 10(d).

Detailed experimental procedures of conducting this experiment using SVR can be found in Supplementary Material, including approaches A and B. The results are depicted for both the train and test phases, according to Table. S5, the proposed SVR method performs slightly better than [18]. Also, SVR-GA significantly outperforms both [33-34], whereas they are based on SVR but without involving parameter optimization. The observation supports the significance of using a genetic algorithm to optimise the model parameters in the proposed method. Due to comparing the performance of both proposed SVR and SVR-GA methods with other relevant techniques, the average R^2 value and RMSE for force estimation were calculated. It was observed that the proposed approach has significantly improved performance measures, which means the automatic selection of parameters (using GA) positively affected SVR parameters optimisation.

Figure. 11: Force signals by applying SVR: (a) Actual and estimated force signals. (b) Error histogram. Force signals by applying SVR-GA: (c) Actual and estimated force signals. (d) Error histogram.

4-2- Impedance identification performance analysis

The mechanical model of the biomechanical joint relates to the measured knee torque sampled at a discrete time step. According to Fig. 1 and Eq. 4, the overall adequate torque would be easily calculated $T_e = F_e L_e$ with the measured force F_e and the active arm length L_e (see Fig. 2(b)). The measure contact force approach takes advantage of the constraints of the apparatus on the human

joint to obtain tonic contractions. Therefore, the authors consider the contact force, limb's dynamics, and time in target data to increase the accuracy of target data.

Studying the human joints' mechanical properties separate the voluntary inputs during natural movements and movements from perturbed joint movements. It is designed to apply unidirectional (flexion) torque perturbations about the knee. In essence, the voluntary movement is not measurable; however, according to Eq. 5, the sum of the EMG-estimated flexion and extension torques provided an estimate of the torque T_0 of the knee, even though EMG's are too noisy to provide reliable information about the voluntary movement. Our use of regularization in the model is critical when the subject is not active.

It is noted that a human joint produces a reaction torque when subjected to a generalized displacement. Therefore, non-zero mechanical impedance should be considered for the biomechanical joint [34]. Section V estimates muscle force reported in Fig. 11 and Supplementary Material. Here, we employed a two-step process: EMG is used to estimate the flexor T_{flex}^{EMG} and extensor T_{ext}^{EMG}. Estimation is obtained using s-EMG from three quadriceps muscles: VM, VL, and RF, with a sampling frequency of 1 kHz. Due to removing baseline noise, measured from a passive (without any joint perturbations) calibration trial was subtracted from the active trials.

Several experimental trials over an operating range are required for impedance characterization. This is one of the main reasons for our robotic design capability. Test trial summary results (mean ± std. dev.) are presented with all subjects and statistically compared at only certain constant torque contraction levels. Attachment inertia based on the active length of the robotic arm is almost 0.4±0.03 kg.m^2. Although limb inertia could be altered with muscle contraction and knee flexion, limb inertia is the difference between total inertia and attachment inertia. According to Table .2, the lower limb inertia estimated in this study (0.486±0.05 kg.m^2) was similar to that reported previously [28].

Table. 3: Inertia measurements and MVC for five subjects

This work set out to evaluate less cumbersome and time-consuming ways to estimate total joint impedance using force/torque estimation. In order to familiarize the subjects with the perturbation and the measurement device, several stimuli were applied (5 ± 0.25 Nm/s) before the measurement was started. In terms of T_P, the IBK model considers only the perturbation joint response. Testing

was performed on the right leg and to avoid anticipation of the stimulus, subjects were visually uncoupled from the perturbation proceeding. The constant level of muscle activation, the device gravity, and the robot dynamic provide the steady-state torques not included. All these steady-state torques should be taken before system identification. A requirement is that the device should be transparent and not affect normal movement when no perturbation is applied.

According to Eq. 13, an initial filter cutoff frequency is determined according to the joint velocity while ensuring that the cutoff frequency does not affect the IBK main parameters estimation. The algorithm of parameter identification is presented based on the formulation in Sec. 3.3 but a step-by-step analysis of the process makes it more understandable. Although one can focus on each component in greater detail, a flowchart in Fig. 12 explains the steps of using the research components in a graphical way as boxes of various tools. The algorithm starts with sEMG signal processing to estimate the purpose of the proposed torque calculation. Start with the purpose of proposed sEMG signal processing in torque calculation. To keep the sequences aligned, it simply represents a map of ordered formulas in the computation process and each step including link motion and measured force is represented by a relevant consideration.

It is coherent with the coding part and consists of implementing the devised algorithm using MATLAB. Following the output of Fig. 12, stiffness and damping could be extracted, but only the stiffness reported in Fig. 13. The estimated stiffness tended to be higher for the first perturbations than others. As it is assumed, it is unrealistic to expect the joint to follow precisely the same trajectory with the same voluntary torque in the perturbed and unperturbed experiments.

Figure. 12: Dynamic parameter identification algorithm.

According to Fig. 14 (a), the zero torque corresponds to the relaxed state. Passive joint stiffness estimated is 33 $Nm.rad^{-1}$ at 60° flexion. Also, in Fig. 14 (b), the passive knee joint damping is 1.74 $Nm\ s\ rad^{-1}$. Although the stiffness relationship became nonlinear in some subjects at the higher background muscle torques, it is noteworthy that joint mechanical impedance is tried to be characterized by stiffness, viscosity, and inertia parameters assuming a linear model. After careful investigations, one linear and 2^{nd} order polynomial are used in the curve fitting for stiffness and damping, respectively. The present study shows systematic knee joint stiffness and viscosity changes with flexor and extensor muscle contraction at joint positions. The result shows that the

stiffness and damping vary with time. Since three subjects are examined in Fig. 14, the impedance does not vary consistently across subjects. After a comparison of the IBK model mechanical parameters, it is noted that the differences in the perturbation method and the nonlinearity in EMG-torque relation during constant-effort contractions are the reasons for the little disagreement.

Figure. 13: Joint stiffness estimation versus time.

Figure. 14: Torque-based model predictions for 3 subjects: (a) stiffness, (b) damping.

5- DISCUSSION AND CONCLUSIONS

Impedance characterization for rehabilitation requires multiple experimental trials over various operating points. It is cumbersome, invasive, time-consuming, and impractical, and this is the main focus of our robot design with the key features and capabilities. A knee rehabilitation robot has been designed based on the impedance estimation from sEMG signals. The manipulator was designed to do more than the typical functions of robotic knee therapy.

This paper focuses on learning algorithms used to encode variable impedance gains for learning, reproduction, and adaptation, regardless of the effect of these gains on robot behavior. The dynamic parameter identification flowchart shows the sequence and interconnection of each part for impedance analysis through logical torque calculation on a single joint axis system. The proposed method includes robot dynamic analysis and force measurement besides the signal processing of sEMG. Analytical torque calculation was performed during the experiment, yet the main challenges appeared in muscle activity considerations. Unlike the traditional representation of EMG-torque relation with a single parameter set for all periods, a time-varying model was simulated using the joint torque as a function of small position perturbations and EMG signal from the joint's muscles. On the other hand, s-EMG is affected by physiological and external factors such as phase neutralization, motion artifacts, ambient noise, and improper placement of electrodes. Therefore, it is imperative to devise suitable pre-processing methods to mitigate the defects of such noises. Due to the level of importance of processing for characterizing, support vector machines and regression have been used for classification and prediction. Knee impedance modulation through force estimation was studied and carried out based on the measured sEMG signals using SVM and SVR. We proposed an intelligent method based on GA to automatically

decide and tune appropriate features and parameters. It was used for both parameter optimisation and also feature selection. Based on the reported results, we have observed that the model based on support vector regression with optimised parameters offers the best performance.

Realizing a safe exploration, the impedance modulation within the proposed estimation techniques increased the accuracy and performance of the therapy. Since muscle models become especially sensitive to tendon stiffness and slack length, the EMG-impedance model could be provided from the EMG without the need for perturbation in the traditional complex procedures. The mechanical parameters of IBK model estimated in this study are generally comparable to those estimated in previous studies. It is noted that the differences in the perturbation method and device may be the reasons for the little disagreement. Also, the other source is the nonlinearity in EMG-torque relation during constant-effort contractions. Nevertheless, EMG was recorded once for the classification; thus, it was unnecessary for further experiments.

For future work, using this embedded platform, we are planning to implement an online model-based impedance estimation that addresses shortcomings for force control instead of using prerecorded sEMG signals. We take the idea a big step further, controlling the robotic therapy by encoding variable impedance gains for robotic learning. The proposed impedance modulation to control strategy can be extended from a broad range of rehabilitation devices to active Orthosis devices.

Disclosure statement:

The authors declare no conflict of interest in preparing this article.

Data availability statement:

The data that support the findings of this study are available from the corresponding author, [Mahdi Bamdad], upon reasonable request.

REFERENCES

[1] Mizrahi, Joseph. "Mechanical impedance and its relations to motor control, limb dynamics, and motion biomechanics." *Journal of medical and biological engineering* 35.1 (2015): 1-20.

[2] Cao, Jinghui, et al. "Control strategies for effective robot assisted gait rehabilitation: the state of art and future prospects." *Medical engineering & physics* 36.12 (2014): 1555-1566.

[3] Gomi, Hiroaki, and Rieko Osu. "Task-dependent viscoelasticity of human multijoint arm and its spatial characteristics for interaction with environments." *Journal of neuroscience* 18.21 (1998): 8965-8978.

[4] Kim, Hyun K., et al. "Estimation of multijoint stiffness using electromyogram and artificial neural network." *IEEE Transactions on Systems, Man, and Cybernetics-Part A: Systems and Humans* 39.5 (2009): 972-980.

[5] Shin, Duk, Jaehyo Kim, and Yasuharu Koike. "A myokinetic arm model for estimating joint torque and stiffness from EMG signals during maintained posture." *Journal of neurophysiology* 101.1 (2009): 387-401.

[6] Disselhorst-Klug, Catherine, Thomas Schmitz-Rode, and Günter Rau. "Surface electromyography and muscle force: Limits in sEMG–force relationship and new approaches for applications." *Clinical biomechanics* 24.3 (2009): 225-235.

[7] Cop, Christopher P., et al. "Unifying system identification and biomechanical formulations for the estimation of muscle, tendon and joint stiffness during human movement." *Progress in Biomedical Engineering* 3.3 (2021): 033002.

[8] Tsuji, Toshio, and Makoto Kaneko. "Noncontact impedance control for redundant manipulators." *IEEE Transactions on Systems, Man, and Cybernetics-Part A: Systems and Humans* 29.2 (1999): 184-193.

[9] Tsuji, Toshio, and Yoshiyuki Tanaka. "Tracking control properties of human-robotic systems based on impedance control." *IEEE Transactions on systems, man, and cybernetics-Part A: Systems and Humans* 35.4 (2005): 523-535.

[10] Bamdad, Mahdi, and Homayoon Zarshenas. "Robotic rehabilitation with the elbow stiffness adjustability." *Modares Mechanical Engineering* 14.11 (2015).

[11] Meng, Wei, et al. "Recent development of mechanisms and control strategies for robot-assisted lower limb rehabilitation." *Mechatronics* 31 (2015): 132-145.

[12] Staudenmann, Didier, et al. “Methodological aspects of SEMG recordings for force estimation–a tutorial and review.” *Journal of electromyography and kinesiology* 20.3 (2010): 375-387.

[13] Liu, Ming Ming, Walter Herzog, and Hans HCM Savelberg. “Dynamic muscle force predictions from EMG: an artificial neural network approach.” *Journal of electromyography and kinesiology* 9.6 (1999): 391-400.

[14] Bai, Fengjun, and Chee-Meng Chew. “Muscle force estimation with surface EMG during dynamic muscle contractions: A wavelet and ANN based approach.” *2013 35th Annual International Conference of the IEEE Engineering in Medicine and Biology Society (EMBC)*. IEEE, 2013.

[15] Choi, Changmok, et al. “Real-time pinch force estimation by surface electromyography using an artificial neural network.” *Medical engineering & physics* 32.5 (2010): 429-436.

[16] Luo, Jing, Chao Liu, and Chenguang Yang. “Estimation of EMG-based force using a neural-network-based approach.” *IEEE Access* 7 (2019): 64856-64865.

[17] Cai, Siqi, et al. “SVM-based classification of sEMG signals for upper-limb self-rehabilitation training.” *Frontiers in Neurorobotics* 13 (2019): 31.

[18] Ibitoye, Morufu Olusola, et al. “SVR modelling of mechanomyographic signals predicts neuromuscular stimulation-evoked knee torque in paralyzed quadriceps muscles undergoing knee extension exercise.” *Computers in biology and medicine* 117 (2020): 103614.

[19] Li, Q. L., Yu Song, and Z. G. Hou. “Estimation of lower limb periodic motions from sEMG using least squares support vector regression.” *Neural Processing Letters* 41.3 (2015): 371-388.

[20] Meng, Wei, et al. “An EMG-based force prediction and control approach for robot-assisted lower limb rehabilitation.” *2014 IEEE International Conference on Systems, Man, and Cybernetics (SMC)*. IEEE, 2014.

[21] Wang, Xinqing, and Juan Gao. “Application of particle swarm optimization for tuning the SVR parameters.” *2015 IEEE International Conference on Advanced Intelligent Mechatronics (AIM)*. IEEE, 2015.

[22] Seel, Thomas, Jörg Raisch, and Thomas Schauer. “IMU-based joint angle measurement for gait analysis.” *Sensors* 14.4 (2014): 6891-6909.

[23] Willemsen, A. Th M., Jan A. van Alste, and H. B. K. Boom. “Real-time gait assessment utilizing a new way of accelerometry.” *Journal of biomechanics* 23.8 (1990): 859-863.

[24] Pedley, Mark. “Tilt sensing using a three-axis accelerometer.” *Freescale semiconductor application note* 1 (2013): 2012-2013.

[25] Kurata, Satoshi, et al. “Joint motion monitoring by accelerometers set at both near sides around the joint.” *Proceedings of the 20th Annual International Conference of the IEEE Engineering in Medicine and Biology Society. Vol. 20 Biomedical Engineering Towards the Year 2000 and Beyond (Cat. No. 98CH36286)*. Vol. 4. IEEE, 1998.

[26] Zhang, Li-Qun, et al. “In vivo human knee joint dynamic properties as functions of muscle contraction and joint position.” *Journal of biomechanics* 31.1 (1997): 71-76.

[27] Tehrani, Ehsan Sobhani, Kian Jalaleddini, and Robert E. Kearney. “Ankle joint intrinsic dynamics is more complex than a mass-spring-damper model.” *IEEE Transactions on Neural Systems and Rehabilitation Engineering* 25.9 (2017): 1568-1580.

[28] Stein, Richard B., et al. “Estimating mechanical parameters of leg segments in individuals with and without physical disabilities.” *IEEE Transactions on Rehabilitation Engineering* 4.3 (1996): 201-211.

[29] Al-Anazi, A. F., and I. D. Gates. “Support vector regression for porosity prediction in a heterogeneous reservoir: A comparative study.” *Computers & Geosciences* 36.12 (2010): 1494-1503.

[30] Vapnik, Vladimir N. “An overview of statistical learning theory.” *IEEE transactions on neural networks* 10.5 (1999): 988-999.

[31] C. H. Wu, G. H. Tzeng, Y. J. Goo, and W. C. Fang, “A real-valued genetic algorithm to optimize the parameters of support vector machine for predicting bankruptcy, “*Expert Syst. Appl.*, vol. 32, no. 2, pp. 397–408, 2007

[32] Gouravaraju, Saipraneeth, Jyotindra Narayan, Roger A. Sauer, and Sachin Singh Gautam. "A Bayesian regularization-backpropagation neural network model for peeling computations." *The Journal of Adhesion* (2021): 1-24.

[33] Fattahi, H., and Babanouri, N. “Applying optimized support vector regression models for prediction of tunnel boring machine performance, “*Geotechnical and Geological Engineering*, *35*(5), (2017): 2205-2217.

[34] Tee, Keng Peng, et al. “Concurrent adaptation of force and impedance in the redundant muscle system.” *Biological cybernetics* 102.1 (2010): 31-44.

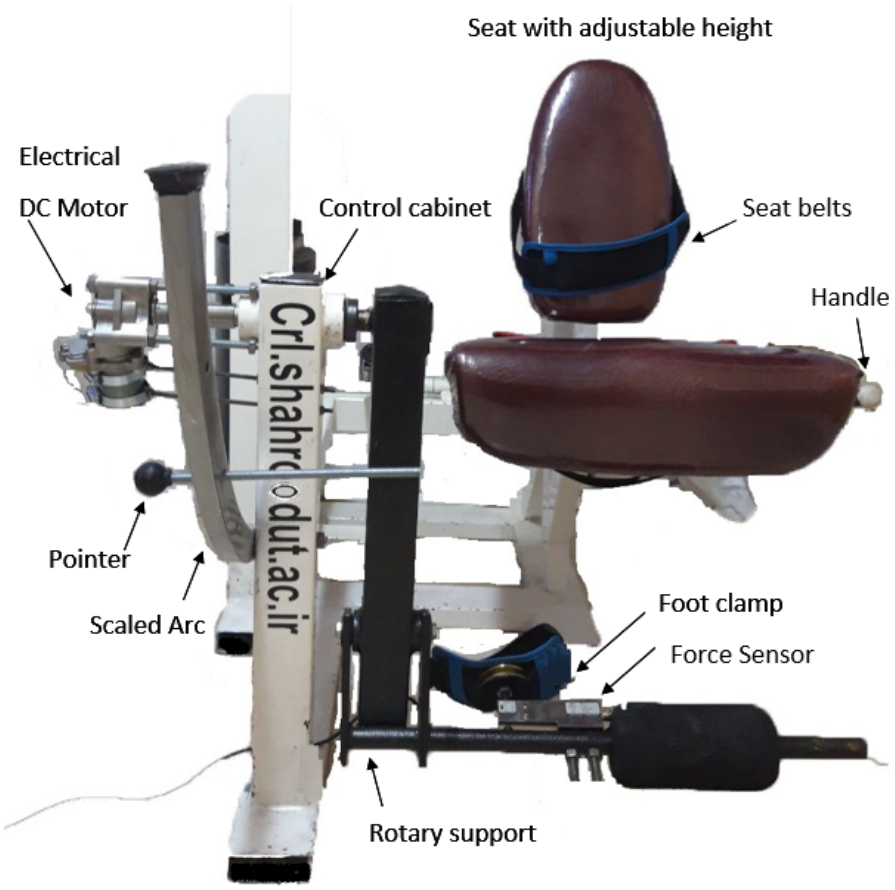

Figure. 5: Device and components- knee rehabilitation robot with annotated details.

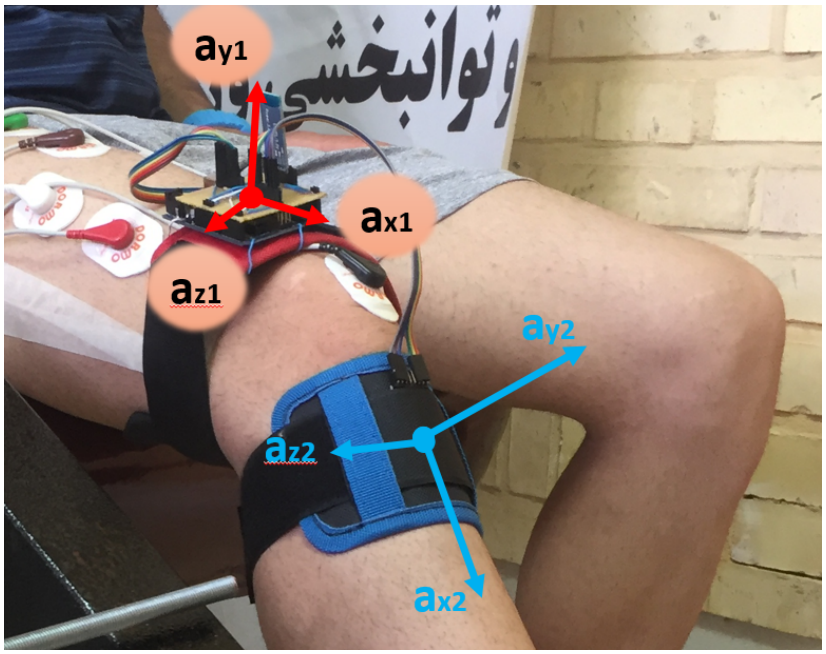

(a)

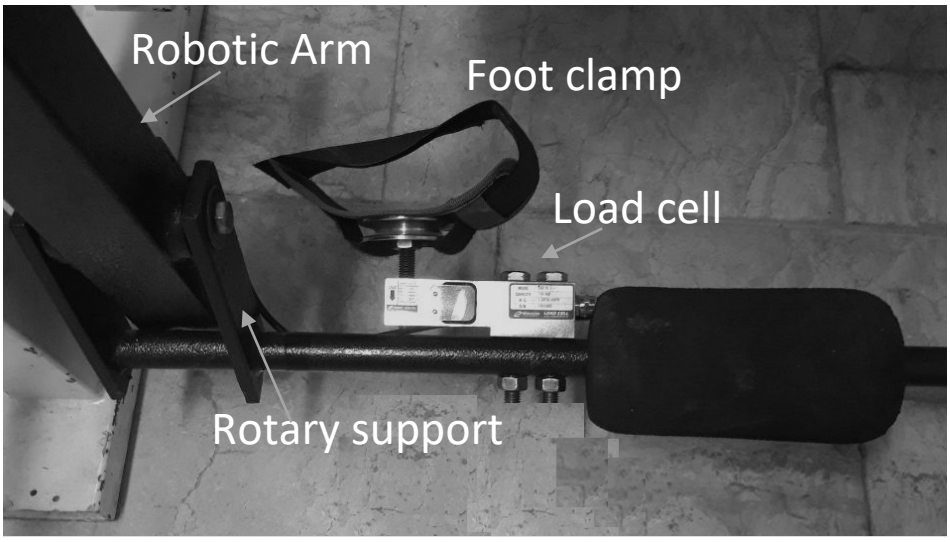

(b)

Figure. 6: The architecture of sensory system (a) wearable IMU arrangement (b) force sensor (load cell).

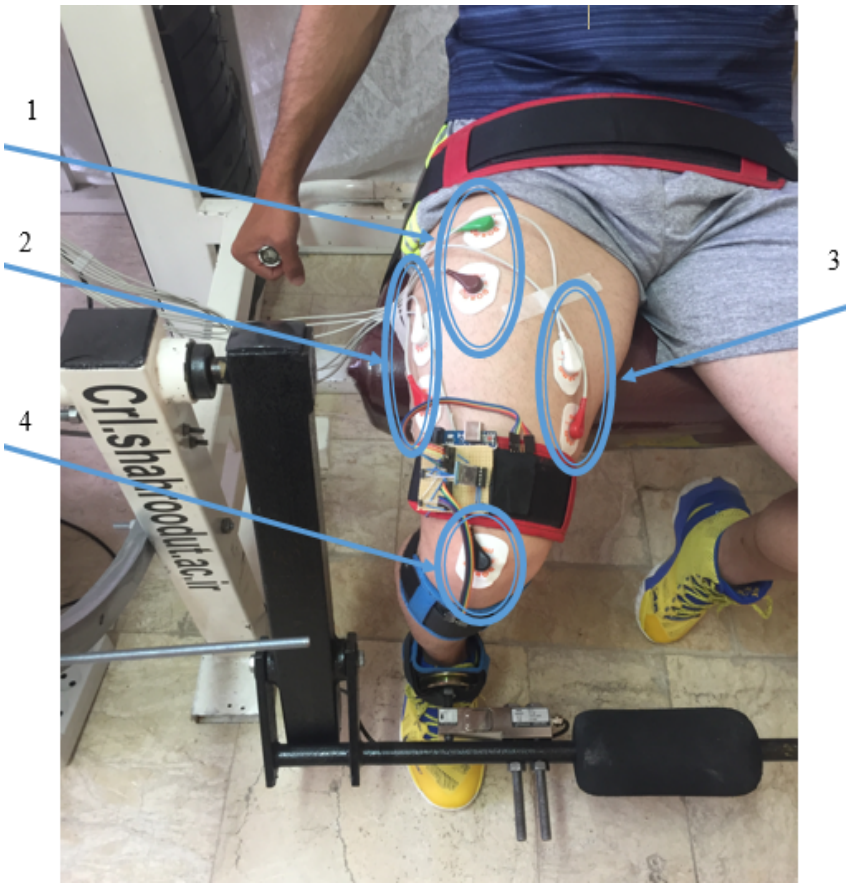

Figure. 7: Electrode locations: (1) Rectus femoris; (2) Vastus medialis; (3) Vastus lateralis; (4) Zero reference electrode.

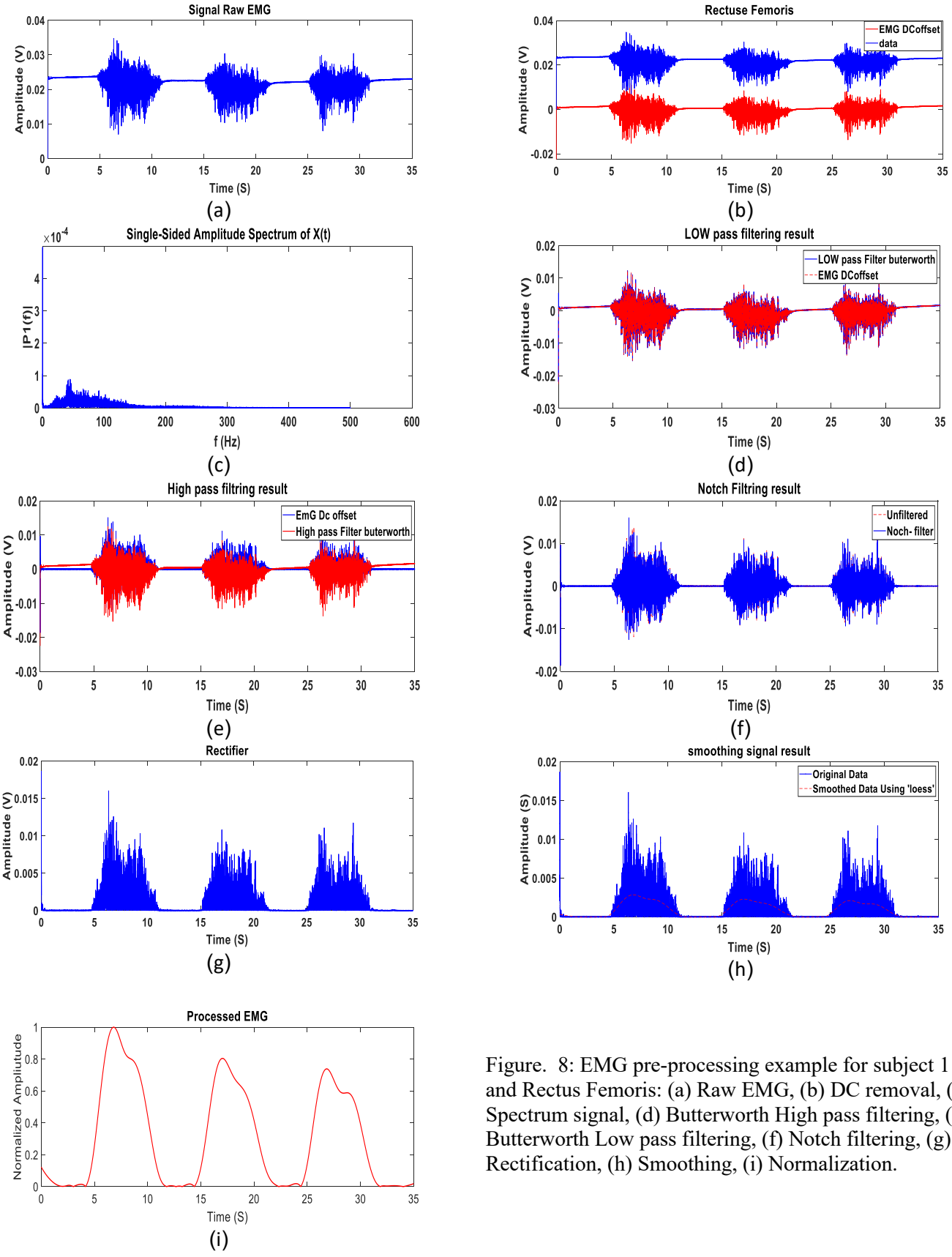

Figure. 8: EMG pre-processing example for subject 1 (S1) and Rectus Femoris: (a) Raw EMG, (b) DC removal, (c) Spectrum signal, (d) Butterworth High pass filtering, (e) Butterworth Low pass filtering, (f) Notch filtering, (g) Rectification, (h) Smoothing, (i) Normalization.

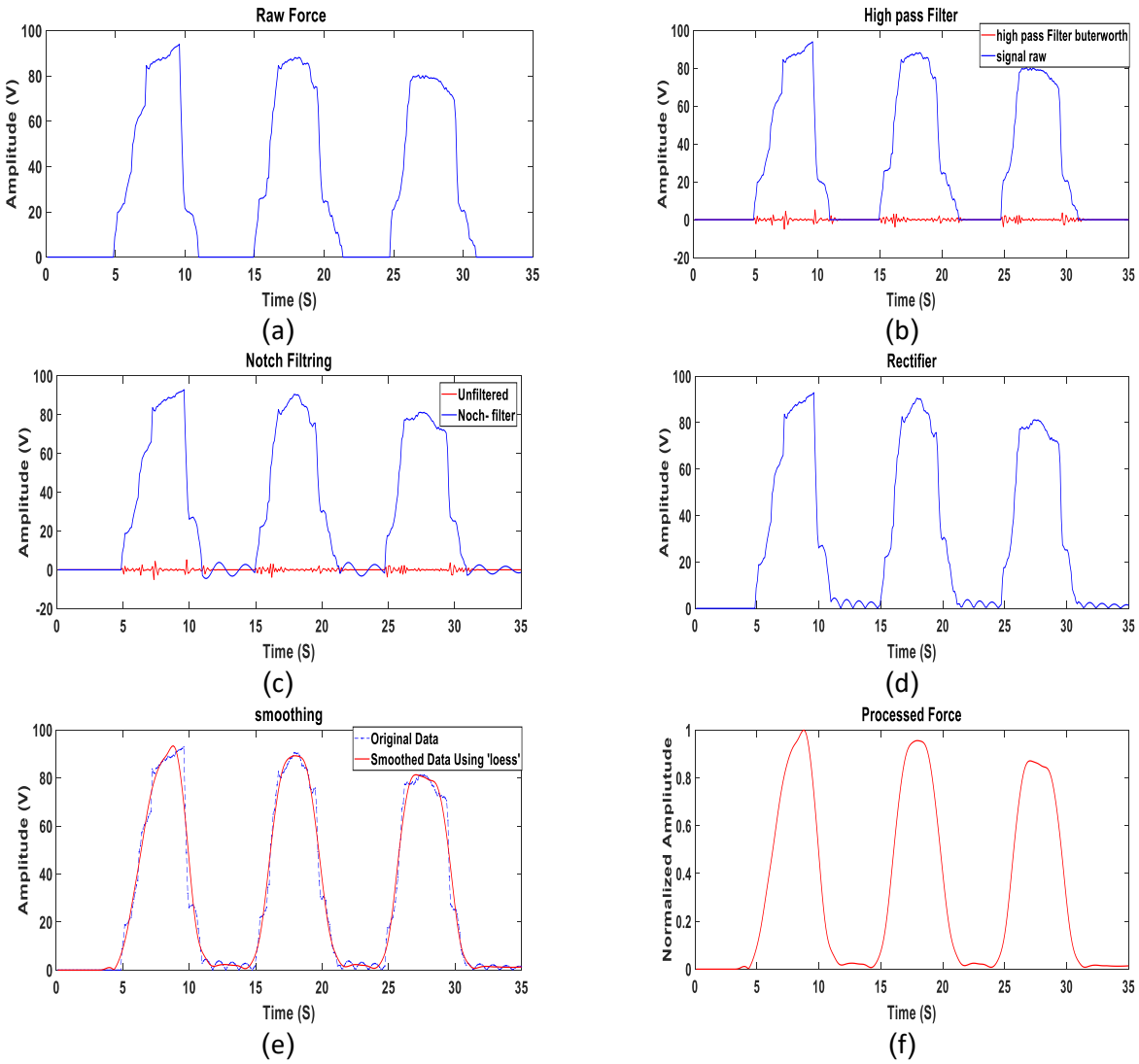

Figure. 5: Force signal pre-processing: (a) Raw signal, (b) Butterworth filtering, (c) Notch filtering, (d) Rectification, (e) Smoothing, (f) Normalization.

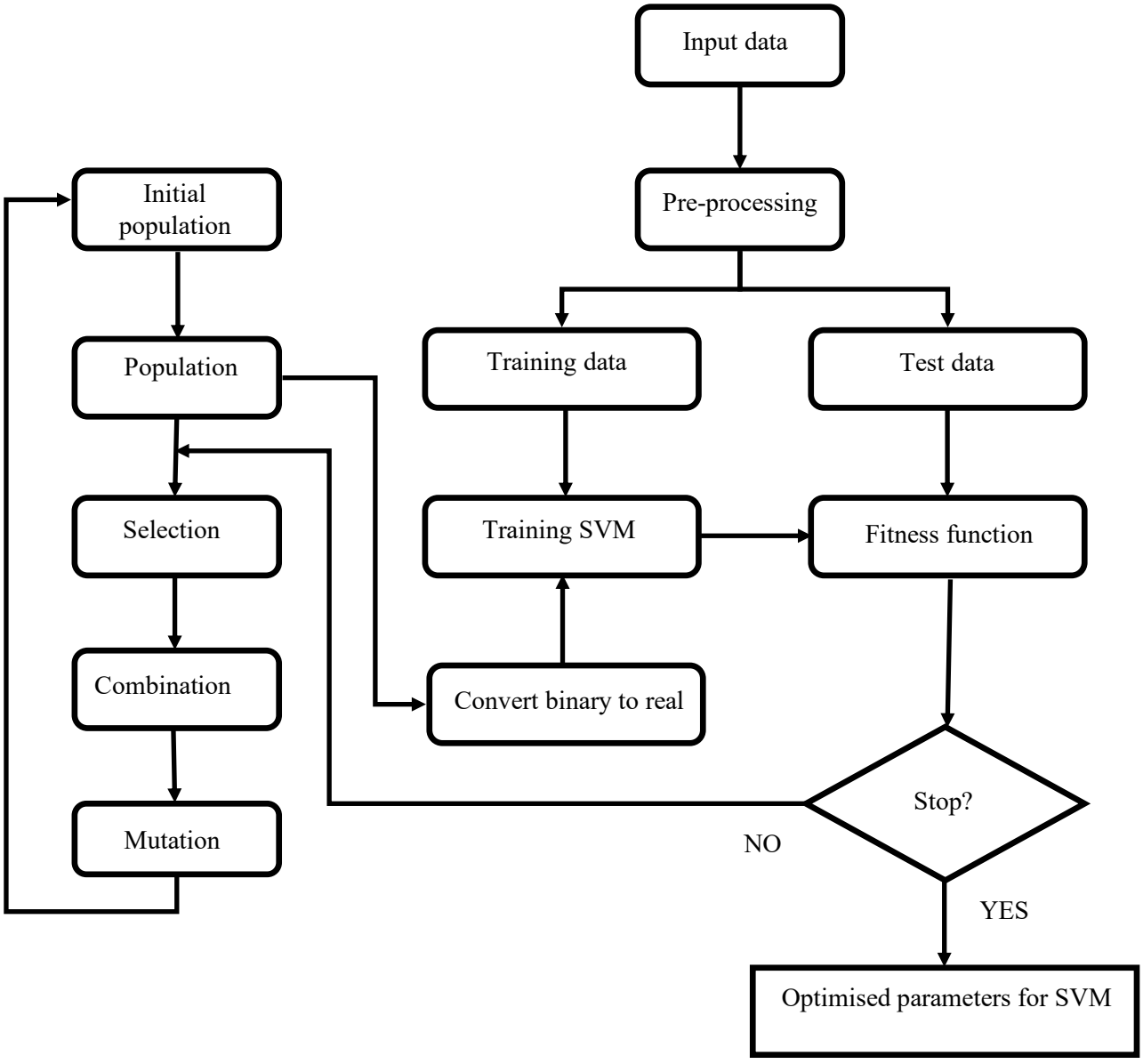

Figure. 6: The proposed flowchart for SVM-GA.

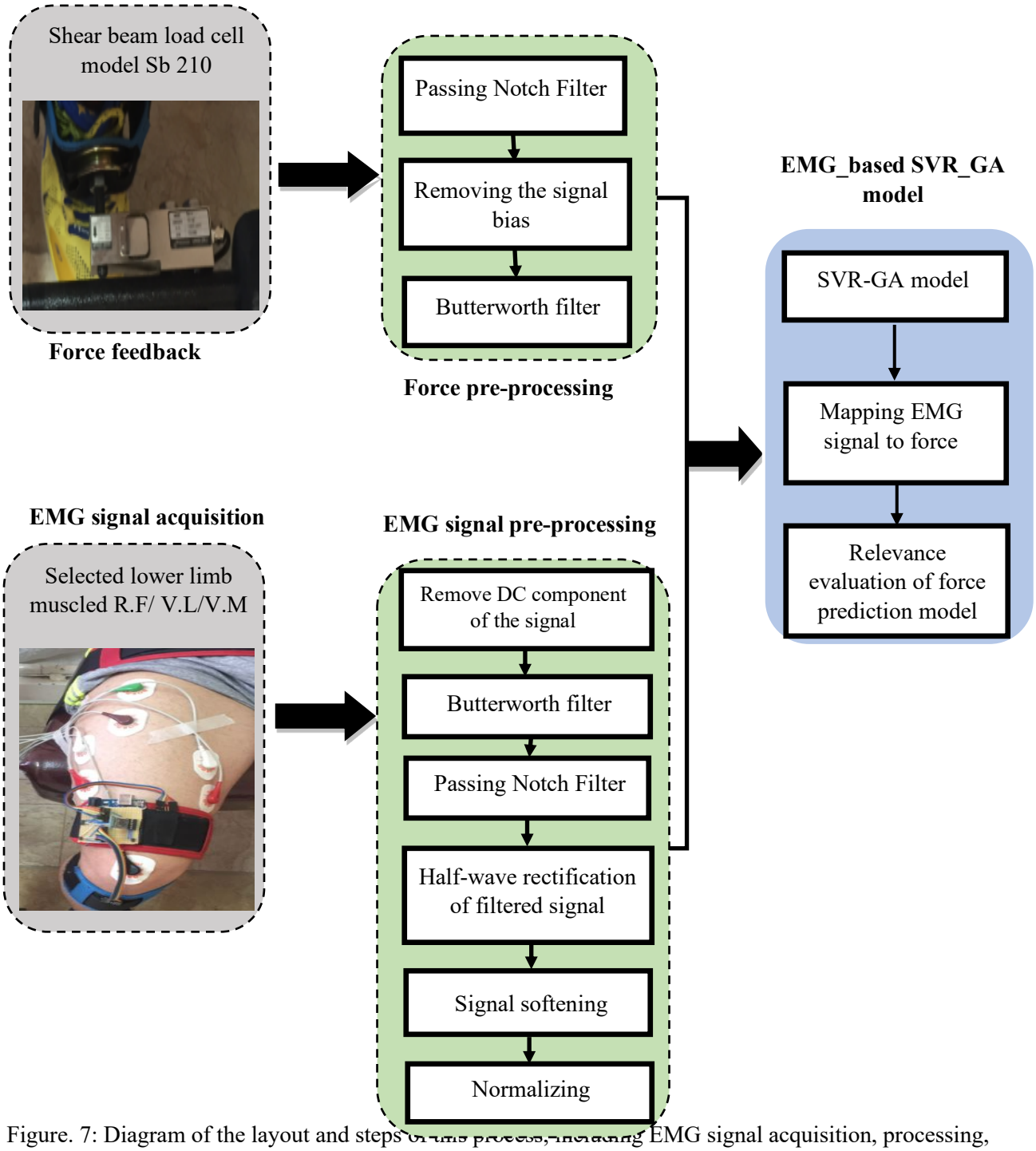

Figure. 7: Diagram of the layout and steps of this process, including EMG signal acquisition, processing, force feedback and the regression model.

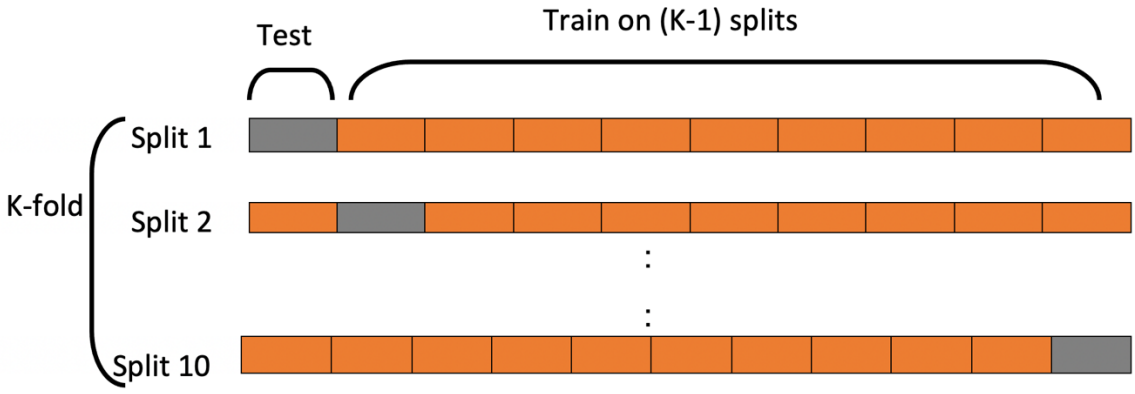

Figure 8: K-fold cross-validation representation with K=10

Table 1: Performance evaluation of the proposed model using 10-fold cross-validation. Each row in the table shows the results when 1 fold is used for testing and the remaining for training.

Split Number	SVM			SVM-GA			SVM-GA-F		
	Accuracy(%)	MSE	RSE	Accuracy(%)	MSE	RSE	Accuracy(%)	MSE	RSE
Split 1	94.81	0.0072	0.0535	95.14	0.0066	0.0486	96.14	0.0053	0.0386
Split 2	90.23	0.0132	0.0978	94.9	0.0069	0.0510	95.25	0.0065	0.0475
Split 3	90.89	0.0132	0.0911	95.32	0.0064	0.0469	96.21	0.0052	0.0379
Split 4	89.88	0.0145	0.1060	95.07	0.0068	0.0493	96.40	0.0049	0.0360
Split 5	94.83	0.0071	0.0538	95.32	0.0065	0.0477	97.28	0.0037	0.0272
Split 6	95.38	0.0061	0.0464	96.0	0.0051	0.0388	95.34	0.0064	0.0466
Split 7	93.64	0.0088	0.0671	94.76	0.0072	0.0524	94.85	0.0071	0.0515
Split 8	91.09	0.0115	0.0876	92.77	0.0092	0.0723	97.81	0.0030	0.0219
Split 9	93.61	0.0087	0.0662	95.13	0.0067	0.0489	95.81	0.0058	0.0419
Split 10	91.0	0.0110	0.0838	94.79	0.0071	0.0521	96.08	0.0054	0.0392

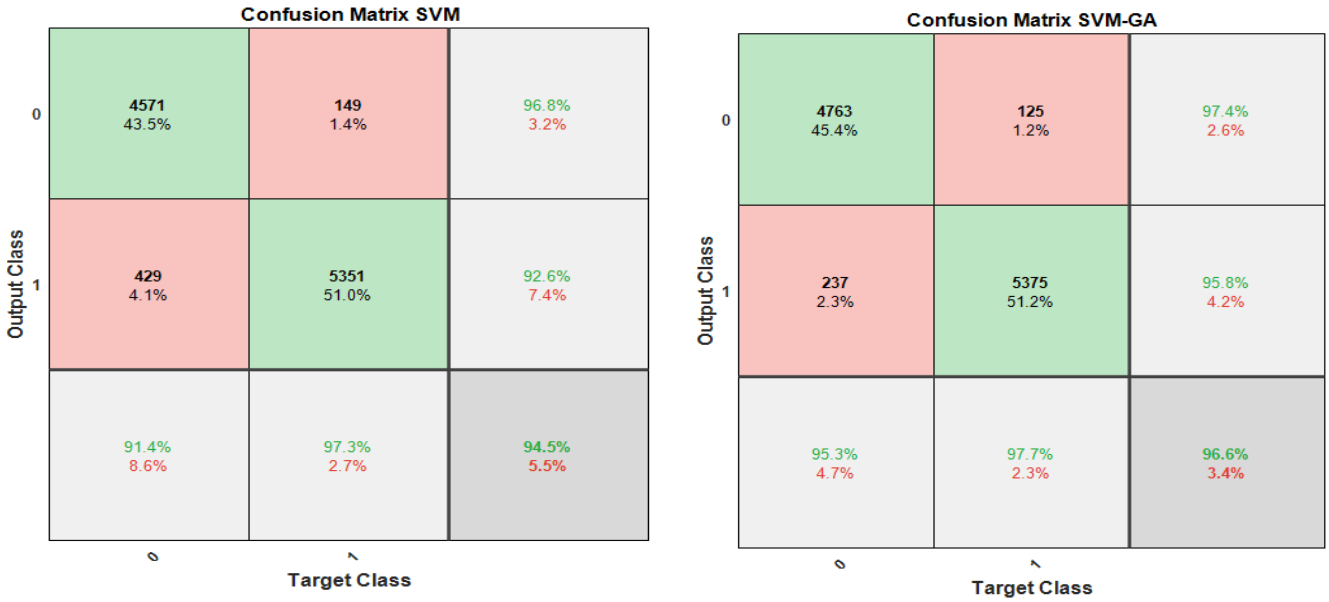

(a) (b)

Figure. 9: Confusion matrix result for S1 with various classification methods.

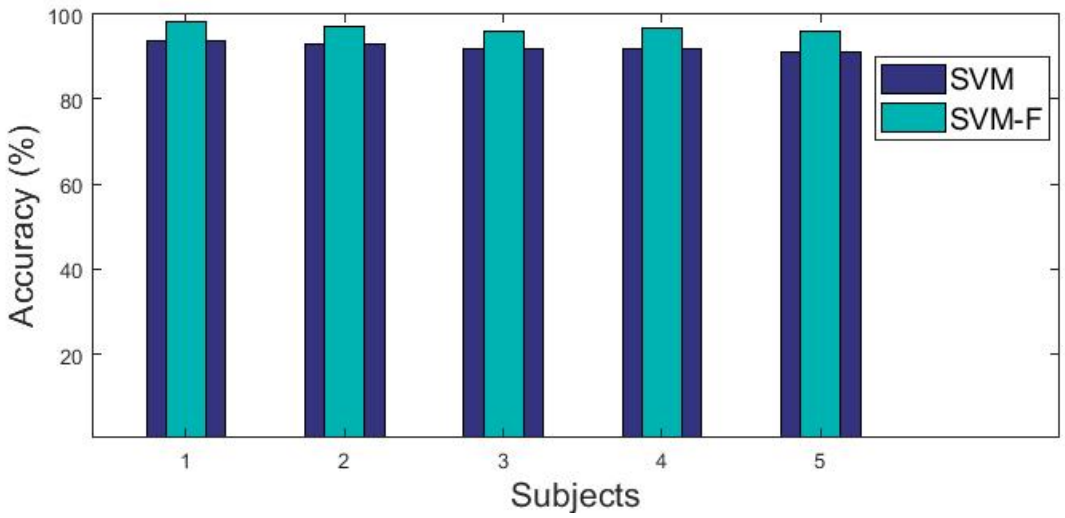

Figure. 10: Comparison of classification accuracy using direct samples (SVM) and selected features (SVM-F).

Table. 2: Classification accuracy all five subjects.

Subject	S1	S2	S3	S4	S5	Average
SVM (%)	94.5	93.1	93.0	92.7	92.4	93.4

SVM-GA (%)	96.6	95.0	94.6	93.2	92.9	94.4
Optimised C , α	2.00 / 1.51	1.86 / 1.22	2.21 / 2.50	1.43 / 1.00	1.79 / 1.90	
SVM-GA-F (%)	98.42	97.1	95.8	96.6	95.9	96.7

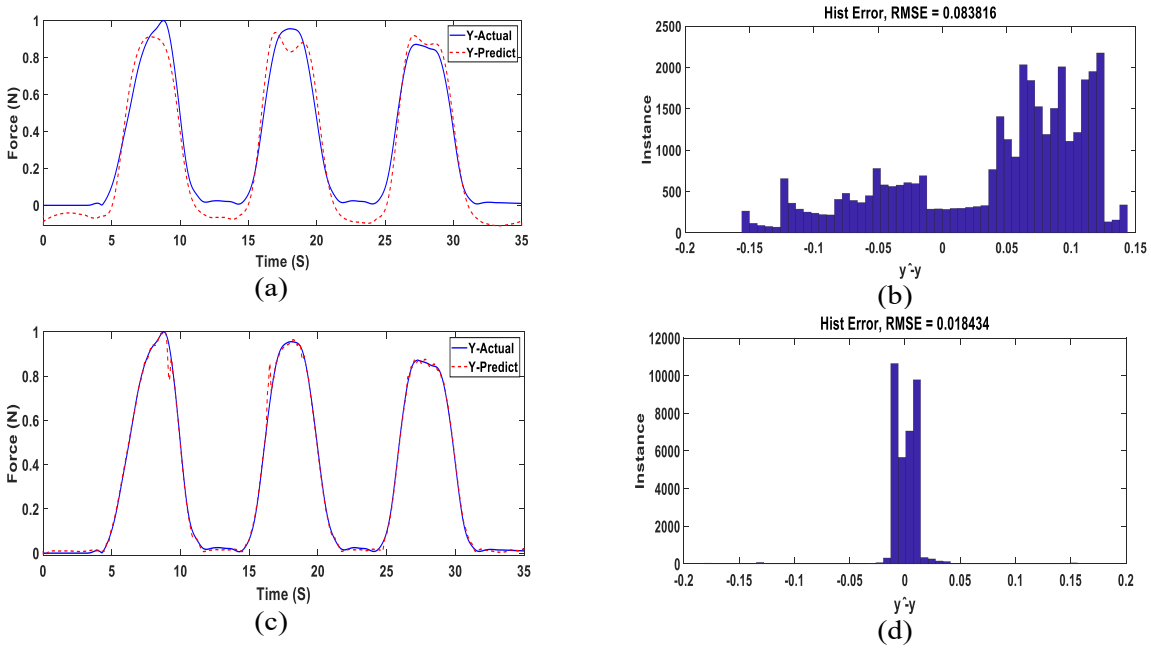

Figure. 11: Force signals by applying SVR: (a) Actual and estimated force signals. (b) Error histogram. Force signals by applying SVR-GA: (c) Actual and estimated force signals. (d) Error histogram.

Table. 3: Inertia measurements and MVC for five subjects

Subject	**Flexion MVC (Nm)**	**Extension MVC (Nm)**	**Total inertia ($kg.m^2$)**
S1	72.5	137.5	0.88
S2	63.0	130	0.85

S3	76	139	0.90
S4	73	122	0.87
S5	97	144	0.93
Mean $\pm \sigma$	76.3±11.23	134.5±7.69	0.886±0.02

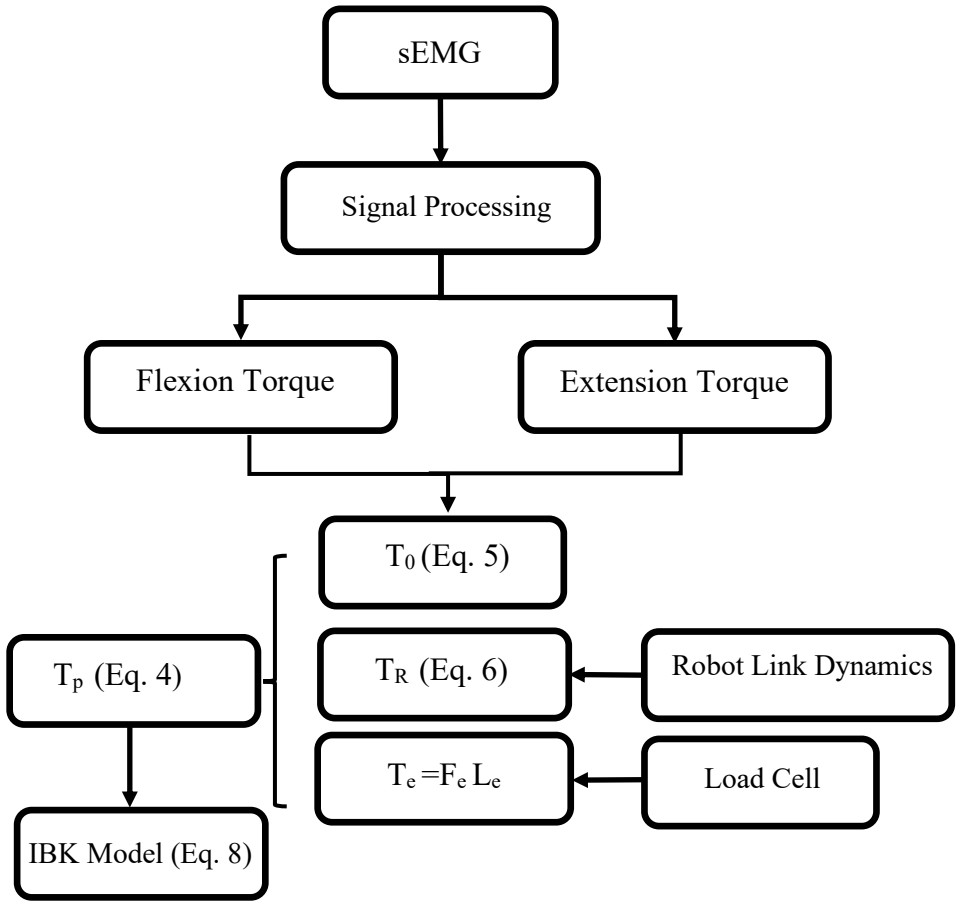

Figure. 12: Dynamic parameter identification algorithm.

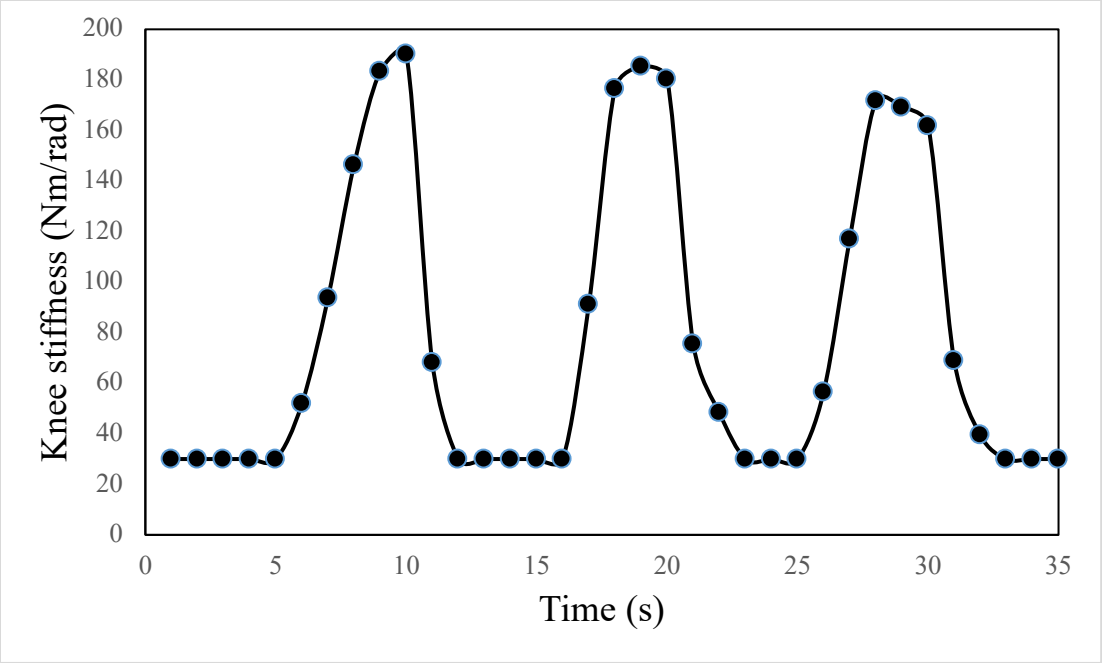

Figure. 13: Joint stiffness estimation versus time.

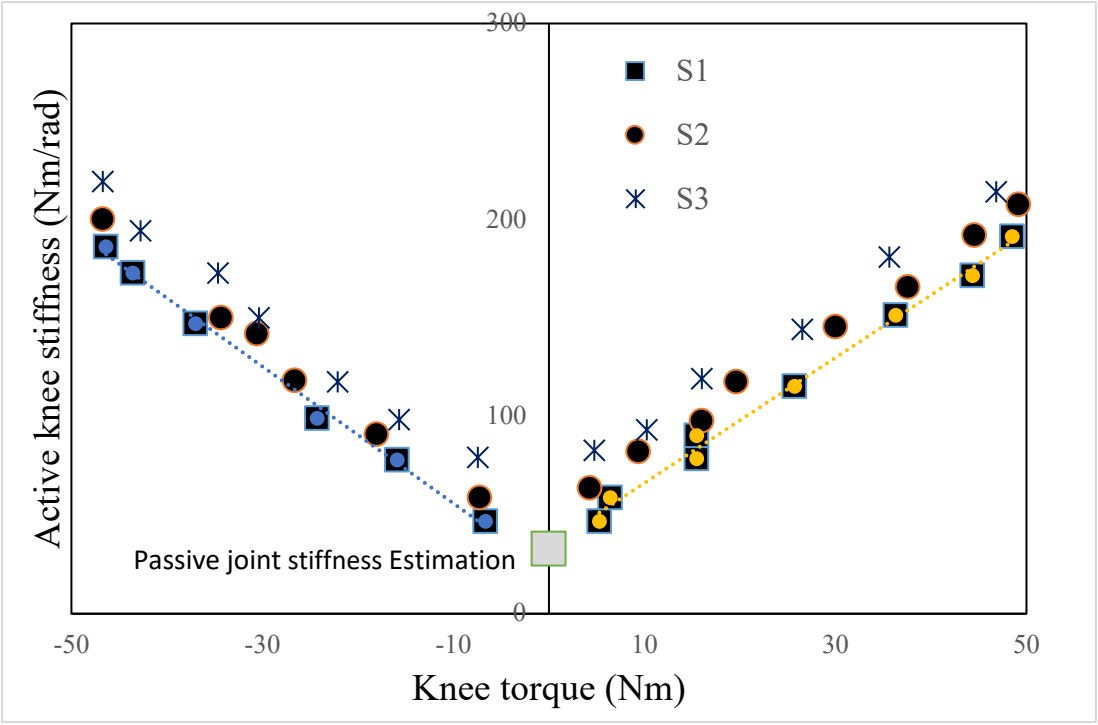

(a)

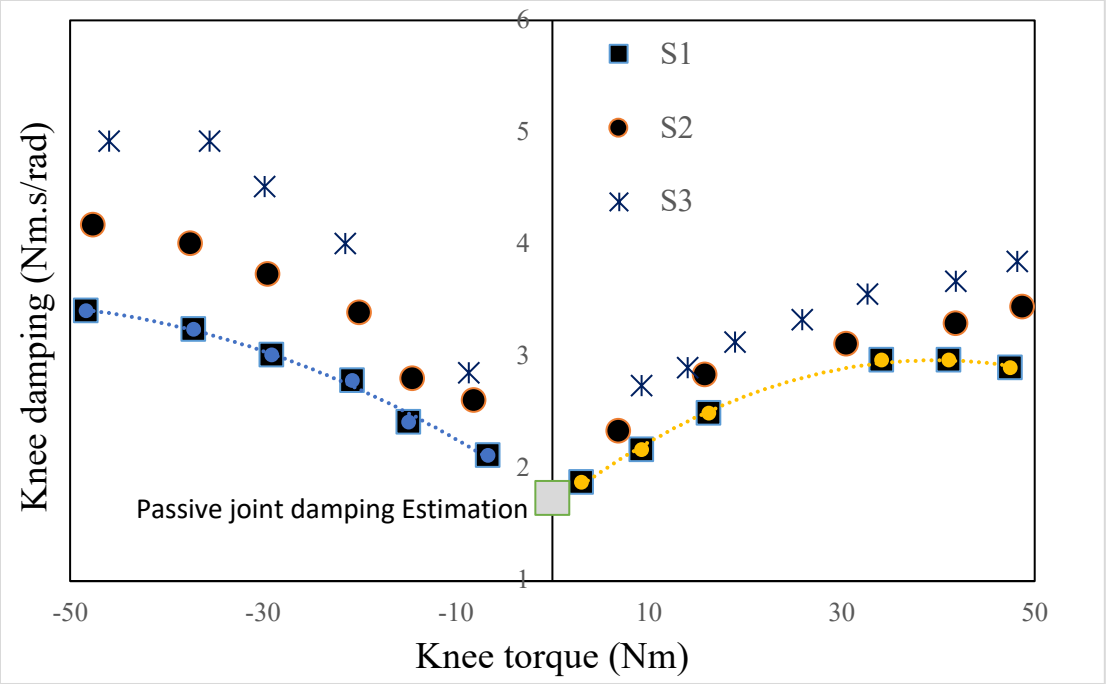

(b)

Figure. 14: Torque-based model predictions for 3 subjects: (a) stiffness, (b) damping.